Molecular Therapy
Methods & Clinical Development
Original Article

A comprehensive study of AAV tropism across C57BL/6 mice, BALB/c mice, and crab-eating macaques

Kailun Fang,[1,4] Xiali Yang,[1,4] Yuanhua Liu,[1] Junhui Xia,[2] Ruoxi Wu,[2] Fan Yang,[1] Canbin Feng,[1] Xinyu Liu,[1] Linyu Shi,[2] Guannan Geng,[1,3] and Hui Yang[1,2]

[1]Institute of Neuroscience, State Key Laboratory of Neuroscience, Key Laboratory of Primate Neurobiology, CAS Center for Excellence in Brain Science and Intelligence Technology, Shanghai Center for Brain Science and Brain-Inspired Intelligence, Shanghai Institutes for Biological Sciences, Chinese Academy of Sciences, Shanghai 200031, China; [2]Huidagene Therapeutics Inc., Shanghai 200131, China; [3]ENT Institute and Department of Otorhinolaryngology, Eye & ENT Hospital, Fudan University, Shanghai 200031, China

Recombinant adeno-associated viruses (AAVs) have been widely used for gene delivery and gene therapy. However, certain AAV serotypes exhibited distinct transduction patterns among different mouse strains or between mice and non-human primates (NHPs). These variations prompted us to investigate the AAV tropism of 21 capsid variants using barcoded AAV libraries among different tissues in C57BL/6 and BALB/c mice, as well as in crab-eating macaques. Our study unveiled that AAV tropisms varied significantly among different mouse strains and species, particularly in capsid variants such as AAV4, AAV9, PHP.B, and CAP-B10. Notably, AAV4 exhibited liver-detargeting properties in both mice and NHPs, and was remarkably efficient in transducing the lung, glomerulus, and pancreatic islet. These findings furnish crucial insights into the variations of AAV tropism among different mouse strains and species and facilitate the selection of appropriate AAV capsids for target tissues among different mouse strains and in NHPs.

INTRODUCTION

Adeno-associated viruses (AAVs) are DNA viruses first identified in rhesus-macaque-kidney cell culture infected with adeno-virus.[1] Over time, multiple wild-type AAV serotypes have been discovered and harnessed for gene delivery and gene therapy, leading to the approval of seven AAV-based drugs.[2–8] Additionally, various engineered AAV capsids have been developed in recent years.[9–18] These capsids exhibit distinct tropisms compared with wild-type capsids, broadening the scope of AAVs for gene delivery.

Due to the variability in tropism among different AAV capsids, exploration of AAV tropism has been undertaken in mice.[19–21] However, certain AAV capsid variants exhibit distinct tropism patterns among C57BL/6 mice, BALB/c mice, and non-human primates (NHPs), complicating the selection of the appropriate capsid across various strains and species.[11,22,23] For instance, AAV-PHP.B exhibits higher transduction efficiency in the CNS of C57BL/6 mice but lower efficiency in BALB/c mice and NHPs.[22] Furthermore, while transgene expression from AAVs remains high and stable in murine livers, vector RNA abundance in primate livers is notably low.[24–27] This inconsistency highlights the crucial need for a comprehensive investigation and comparison of AAV tropism across different mouse strains and NHPs.

In our study, we constructed barcoded AAV libraries comprising 21 capsid variants, including AAV1-AAV9, rh10, rh74, DJ, i.e., LK03, B1, HSC15, PHP.B, PHP.eB, PHP.S, CAP-B10, and MyoAAV-2A, to explore the differences in AAV tropism across species. These AAV libraries were administered intravenously to C57BL6 mice, BALB/c mice, and NHPs. At 3 weeks after injection, we evaluated the DNA and RNA abundance of each tissue using qPCR and barcode sequencing. Significant variations in AAV tropisms were observed between the two mouse strains and between mice and NHPs. These findings offer valuable insights into AAV tropism variations across strains and species, facilitating the selection of appropriate AAV capsids for target tissues in both mice and crab-eating macaques.

RESULTS

Construction of barcoded AAV libraries containing 21 capsids

To explore the diverse AAV tropisms across C57BL/6 mice, BALB/c mice, and crab-eating macaques, we adopted a barcode-sequencing

Received 28 April 2024; accepted 11 February 2025;
https://doi.org/10.1016/j.omtm.2025.101434.

[4]These authors contributed equally

Correspondence: Guannan Geng, Institute of Neuroscience, State Key Laboratory of Neuroscience, Key Laboratory of Primate Neurobiology, CAS Center for Excellence in Brain Science and Intelligence Technology, Shanghai Research Center for Brain Science and Brain-Inspired Intelligence, Shanghai Institutes for Biological Sciences, Chinese Academy of Sciences, Shanghai 200031, China.
E-mail: jsyxggn@163.com
Correspondence: Hui Yang, Institute of Neuroscience, State Key Laboratory of Neuroscience, Key Laboratory of Primate Neurobiology, CAS Center for Excellence in Brain Science and Intelligence Technology, Shanghai Research Center for Brain Science and Brain-Inspired Intelligence, Shanghai Institutes for Biological Sciences, Chinese Academy of Sciences, Shanghai 200031, China.
E-mail: huiyang@ion.ac.cn

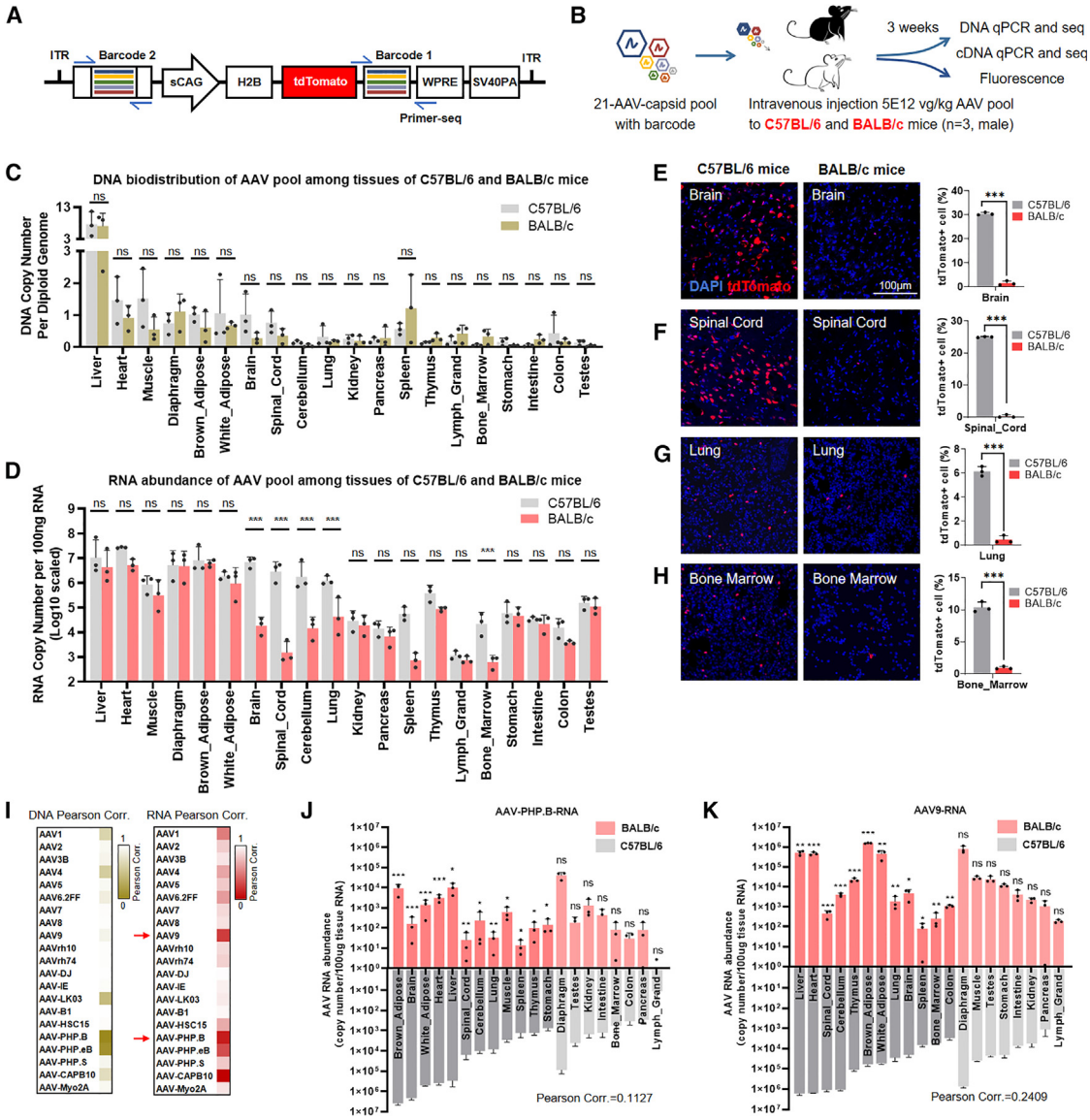

Figure 1. AAV transduction differences between C57BL/6 and BALB/c mice

(A) Schematic of the AAV constructs containing two sets of 7nt-barcodes. (B) Schematic of the AAV tropism analysis procedure in C57BL/6 and BALB/c mice. We injected 5E12 vg/kg AAV pool intravenously into mice (N = 3). The infection and transduction efficiency of AAV library was assessed at the DNA, RNA, and protein levels. (C) Quantitative analysis of vector DNA abundance of overall AAV pools in C57BL/6 and BALB/c mice using qPCR. Vector copy numbers were normalized to per diploid genome using the mouse Gapdh gene as a control. N = 3; means ± SD; ns, not significant; unpaired t tests. (D) Quantitative analysis of the AAV RNA abundance of overall AAV pools between C57BL/6 and BALB/c mice. N = 3; means ± SD; ns, not significant; ***$p < 0.001$; unpaired t tests. (E–H) Representative images of tdTomato expression in tissues of the brain (E), spinal cord (F), lung (G), and bone marrow (H). The right graph shows the quantification of tdTomato$^+$ cells among all cells. N = 3; means ± SD; ***$p < 0.001$; unpaired t tests. (I) Pearson correlation elucidating the variation of the transduction pattern of each capsid between C57BL/6 and BALB/c mice. (J and K) Quantitative analysis of the AAV RNA abundance of AAV-PHP.B (J) or AAV9 (K) in C57BL/c and BALB/c mice. N = 3; means ± SD; ***$p < 0.001$; unpaired t tests.

method.[19,20,28,29] Specifically, we designed a series of barcoded constructs termed Barcode2-CAG-H2B-tdTomato-WPRE-Barcode1-SV40polyA. Each pair of Barcode1 and Barcode2 consists of distinct 7-mer identifiers representing individual AAV capsids and enabling the assessment of potential sequencing bias (Figure 1A). We explored 21 AAV capsids in our study, including AAV1-AAV9, rh10, rh74, DJ, i.e., LK03, B1, HSC15, PHP.B, PHP.eB, PHP.S, CAP-B10, and MyoAAV-2A (materials and methods). Each capsid variant was packaged with one barcoded construct. Subsequently, all AAV capsid variants were mixed into two parallel libraries for tropism assessment in mice and macaques (Figures S1A and S1B). We gauged the relative abundance of each capsid in the AAV library by analyzing the

abundance of the respective barcodes. Sequencing results of the AAV libraries displayed consistency between Barcode1 and Barcode2 (Figures S1C and S1D), indicating that there was no PCR amplification bias stemming from differing barcode sequences. We applied Barcode1 in the next study.

AAV transduction was different between C57BL6 and BALB/c mice

Next, we explored the potential differences in AAV tropism between two mouse strains. Specifically, we administrated the AAV library intravenously at a total dose of 5E12 vg/kg to 5-week-old male C57BL/6 mice and BALB/c mice (N = 3 per group). After 3 weeks, we collected 20 mouse tissues to investigate AAV tropism at the DNA, RNA, and protein levels (Figure 1B). The biodistribution of vector DNA and RNA abundance of pooled AAV were evaluated by qPCR. Although we observed no significant difference in vector DNA abundances between BALB/c and C57BL/6 mice (Figure 1C), we found mRNA abundance in certain BALB/c mouse tissues, including the brain, spinal cord, cerebellum, lung, and bone marrow, that was notably lower compared with C57BL/6 mice (Figure 1D). To validate these findings, we examined the tdTomato signal in tissues and noted significant transcriptional variation between the two strains. The percentage of tdTomato$^+$ cells was significantly reduced in BALB/c mice compared with C57BL/6 mice in the brain (30.45% ± 0.56% vs. 1.51% ± 0.93%; $p < 0.0001$) (Figure 1E), spinal cord (66.50% ± 2.42% vs. 0.33% ± 0.18%; $p < 0.0001$) (Figure 1F), lung (6.14% ± 0.40% vs. 0.45% ± 0.33%; $p < 0.0001$) (Figure 1G), and bone marrow (10.40% ± 0.82% vs. 0.93% ± 0.22%; $p < 0.0001$) (Figure 1H). Overall, these findings suggest differential transduction efficiency of pooled AAVs between BALB/c and C57BL/6 mice, particularly evident in the CNS, lung, and bone marrow.

Moreover, we assessed the differences in tropism among each AAV capsid variant between the two mouse strains. Using barcode sequencing of barcode 1, we dissected the vector DNA and RNA abundance of each capsid from pooled AAVs in both C57BL/6 mice (Figures S2A and S2B) and BALB/c mice (Figures S3A and S3B). Subsequently, we compared the transduction patterns for each AAV capsid between mouse strains using Pearson correlation coefficients. Several capsid variants, including AAV9, PHP.B, PHP.eB, and CAP-B10, exhibited the greatest variations in transduction patterns between C57BL/6 and BALB/c mice (Figure 1I). For instance, AAV-PHP.B, an engineered capsid derived from AAV9,[14] demonstrated distinct transduction patterns in BALB/c mice compared with C57BL/6 mice (Pearson correlation coefficient = 0.1127). The transduction efficiency of AAV-PHP.B in the CNS of BALB/c mice was lower compared with C57BL/6 mice, which is consistent with prior findings.[22] Furthermore, we observed that the reduction of transduction efficiency of AAV-PHP.B was not restricted to the nervous system of BALB/c mice, but also in other tissues, including the liver, heart, adipose tissue, and lungs (Figure 1K), which indicates an overall reduction of AAV-PHP.B transduction in BALB/c mice. Additionally, AAV9, the parental capsid of PHP.B, also exhibited a broader reduction in transgene expression efficiency in most tissues in BALB/c mice compared with C57BL/6 mice (Figure 1J). These results collectively highlight that the tropism of certain AAV capsids may vary across different mouse strains.

AAV transduction was different between C57BL/6 mice and crab-eating macaques

To further assess the tropism variation across species, we investigated AAV transduction efficiency in mice and macaques. We administered a single dose of 5E12 vg/kg of pooled AAVs to male crab-eating macaques (N = 3) via intravenous injection. The pre-existing neutralizing antibody (NAb) against several types of AAV capsids (AAV2, AAV5, AAV8, and AAV9) was estimated before AAV library injection using Luciferase assay. One macaque exhibited AAV2 NAb titer over 1/660 and all three macaques exhibited AAV8 NAb titer over 1/66 (Table S1). Due to the unavailability of selecting macaques without pre-existing antibodies against multiple AAV capsids in macaques and the potential adaptive immune response after AAV infusion could be high, we implemented a g3T cell and B cell suppression regimen (2 mg/kg rapamycin daily[30] and 20 mg/kg rituximab weekly[31,32]) to suppress the anti-capsid or anti-transgene immune response. The NAb titer of several capsids (e.g., AAV2, AAV5, AAV8, and AAV9) after injection was equal or lower compared with the titer before AAV library infusion (Table S1), implying some extent of immune suppression. At 3 weeks after injection, we euthanized these macaques and collected 28 tissues for evaluating AAV transduction efficiency (Figure 2A). The vector DNA abundance of pooled AAVs was comparable with that in C57BL/6 mice in most tissues (Figure 2B). However, the RNA abundance of pooled AAVs was significantly lower in 20 of 28 tissues compared with C57BL/6 mice (Figure 2C). We confirmed these results by examining the tdTomato signal in different tissue sections. The tdTomato staining in macaques was significantly lower in the liver (66.50% ± 2.42% vs. 0.33% ± 0.18%; $p < 0.0001$) (Figure 2D), heart (54.45% ± 2.75% vs. 7.83% ± 1.44%; $p < 0.0001$) (Figure 2E), muscle (79.51% ± 2.30% vs. 33.60% ± 8.36%; $p < 0.0001$) (Figure 2F), and midbrain (30.45% ± 0.56% vs. 5.98% ± 1.20%; $p < 0.0001$) (Figure 2G). Overall, transduction efficiencies of pooled AAVs were lower in crab-eating macaques than in C57BL/6 mice at both the RNA and protein levels.

Furthermore, we compared the transduction patterns of different capsid variants between C57BL/6 mice and crab-eating macaques. The abundance of vector DNA and RNA for each capsid was calculated and analyzed from pooled AAV data (Figures 3A and 3B). Among all tested capsids, AAVs such as AAV4, AAV5, PHP.B, PHP.eB, CAP-B10, and MyoAAV-2A exhibited high transduction variations between mice and macaques (Figure 3C). For instance, the transduction efficiency of AAV4 in various tissues of C57BL/6 mice showed higher levels in the liver, lung, heart, muscle, and adipose tissues and exhibited lower levels in other tissues. However, in macaques, the overall transduction pattern of AAV4 was uniform and low, indicating distinct tropism patterns from mice (Figure 3D). Similar tropism variations were also observed in AAV-CAP.B10 between C57BL/6 mice and crab-eating macaques (Figure 3E). These findings underscore differences in tropism among different species,

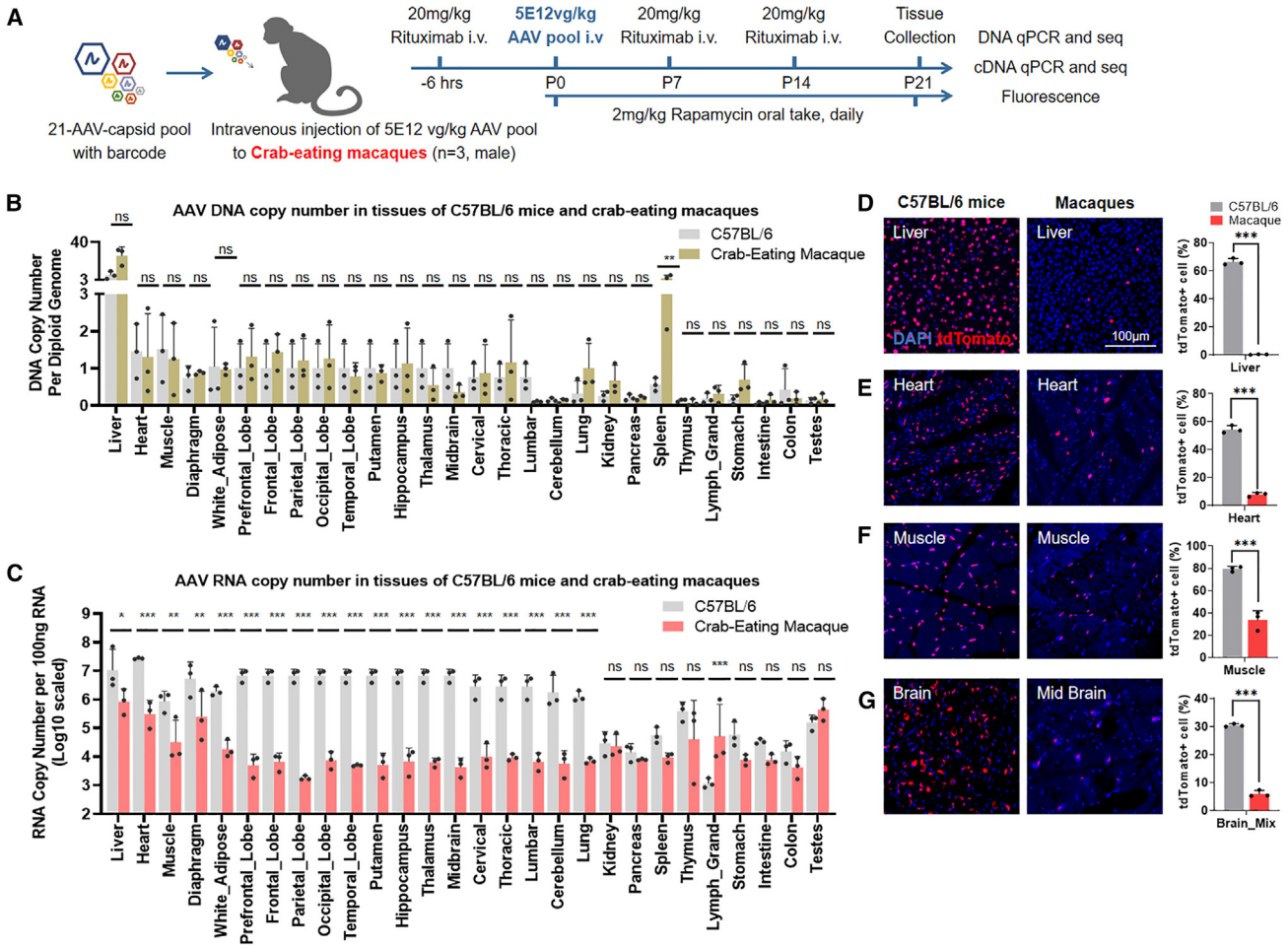

Figure 2. Overall AAV transduction differences between C57BL/6 mice and crab-eating macaques

(A) Schematic of the AAV tropism analysis procedure in crab-eating macaques. We injected 5E12 vg/kg AAV pool intravenously to macaques (N = 3, male). Rituximab and rapamycin were applied to suppress the potential immune response. The infection and transduction efficiency of AAV pool was assessed at the DNA, RNA, and protein levels. (B) Quantitative analysis of the vector DNA abundance of overall pooled AAVs in C57BL/6 mouse and crab-eating macaques using qPCR. Vector copy numbers were normalized to per diploid genome using mouse or macaque Gapdh gene as an internal control. N = 3; means ± SD; ns, not significant; $^{**}p < 0.01$; unpaired t tests. (C) Quantitative analysis of AAV RNA abundance of overall AAV library between C57BL/6 mice and crab-eating macaques. N = 3; means ± SD; ns, not significant; $^{*}p < 0.05$; $^{**}p < 0.01$; $^{***}p < 0.001$; unpaired t tests. (D–G) Representative images of tdTomato expression in tissues including liver (D), heart (E), muscle (F), and brain (G). The right graph shows the quantification of tdTomato^{+} cells among all cells. N = 3; means ± SD; $^{***}p < 0.001$; unpaired t tests. The data and the brain section in C57BL/6 mice in Figure 2G were the same as in Figure 1E.

emphasizing that conclusions drawn from one mouse strain may not be transferable to macaques without further validation.

Selection of the most efficient AAV capsids in specific tissues across strains and species

Having assessed the transduction efficiency of 21 capsids, we were able to identify the most suitable AAV capsids for targeting specific tissues across species. The top five capsids with the greatest transduction efficiency in each specific tissue in C57BL/6 mice, BALB/c mice, and crab-eating macaques were ranked accordingly. Capsids demonstrating high transduction efficiency in both mice and NHPs were highlighted.

In our findings, AAVrh10 and AAVrh74 emerged as the most effective capsids for transducing the liver in both mice and macaques (Figure 4A). However, it is important to note that certain capsids recognized for their liver-tropic characteristics struggled to effectively transduce the liver across species.[9,11] For instance, AAV-DJ displayed high transduction efficiency only in mice, and AAV6.2FF and LK03 showed strong liver tropism exclusively in macaques (Figure 4A). For transduction in muscle, heart, and diaphragm, MyoAAV-2A demonstrated the greatest efficiency in both mice and macaques. AAV9 and AAVHSC15 exhibited notable muscle tropism as well (Figures 4B, S4A, and S4B). Moreover, the CNS is another significant target in AAV-mediated gene therapy. Among the 21 capsids, AAV9

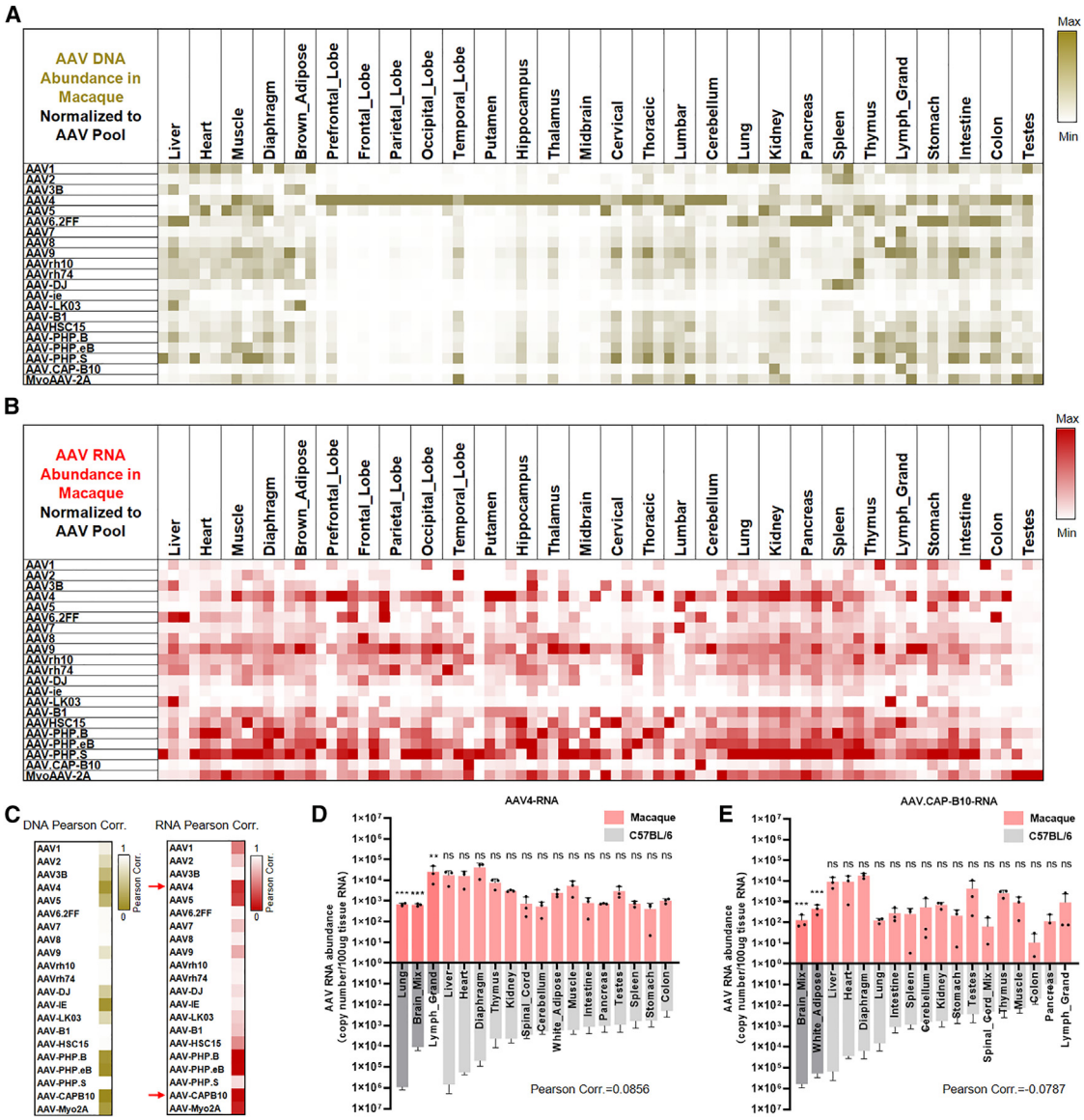

Figure 3. AAV transduction differences of each capsid between C57BL/6 mice and crab-eating macaques

(A) Heatmap of AAV DNA abundance of each serotype in each crab-eating macaque (N = 3). The DNA abundance of each capsid was calculated from the total DNA abundance of the pooled AAVs and the proportion of each capsid. Every three cells in the heatmap represents independent data from three individual macaques to show variation between animals. (B) Heatmap of AAV RNA abundance of each serotype in each crab-eating macaque (N = 3). (C) Pearson correlation elucidating the variation of transduction pattern in each capsid between C57BL/6 mice and crab-eating macaques. (D and E) Quantitative analysis of AAV RNA abundance of AAV4 (D) or AAV.CAP-B10 (E) in C57BL/c mice and crab-eating macaques.

N = 3; means ± SD; ns, not significant; $^{**}p < 0.01$; $^{***}p < 0.001$; unpaired t tests.

and PHP.S showed the greatest efficiency for brain transduction in both mice and macaques. Interestingly, some capsid variants engineered from AAV9 to enhance their neurotropism, such as PHP.B, PHP.eB, and CAP-B10, did not exhibit improvement but also no apparent decrease in transduction compared with AAV9 in the macaque brain, cerebellum, and spinal cord in our findings (Figures 4C, S4C, and S4D).

Furthermore, we delved into the transduction efficiency of capsids in tissues that have not received extensive attention in previous studies. Among the tested capsid variants, AAV4 emerged as the most efficient capsid for gene delivery in the lung, kidney, and pancreas in both mice and macaques (Figures 4D, 4F, and 4G). AAV9, in contrast, proved to be the most efficient capsid for gene delivery to the pancreas, stomach, intestine, colon, and testes (Figures 4E, 4G, 4H, S4G, and S4H). In

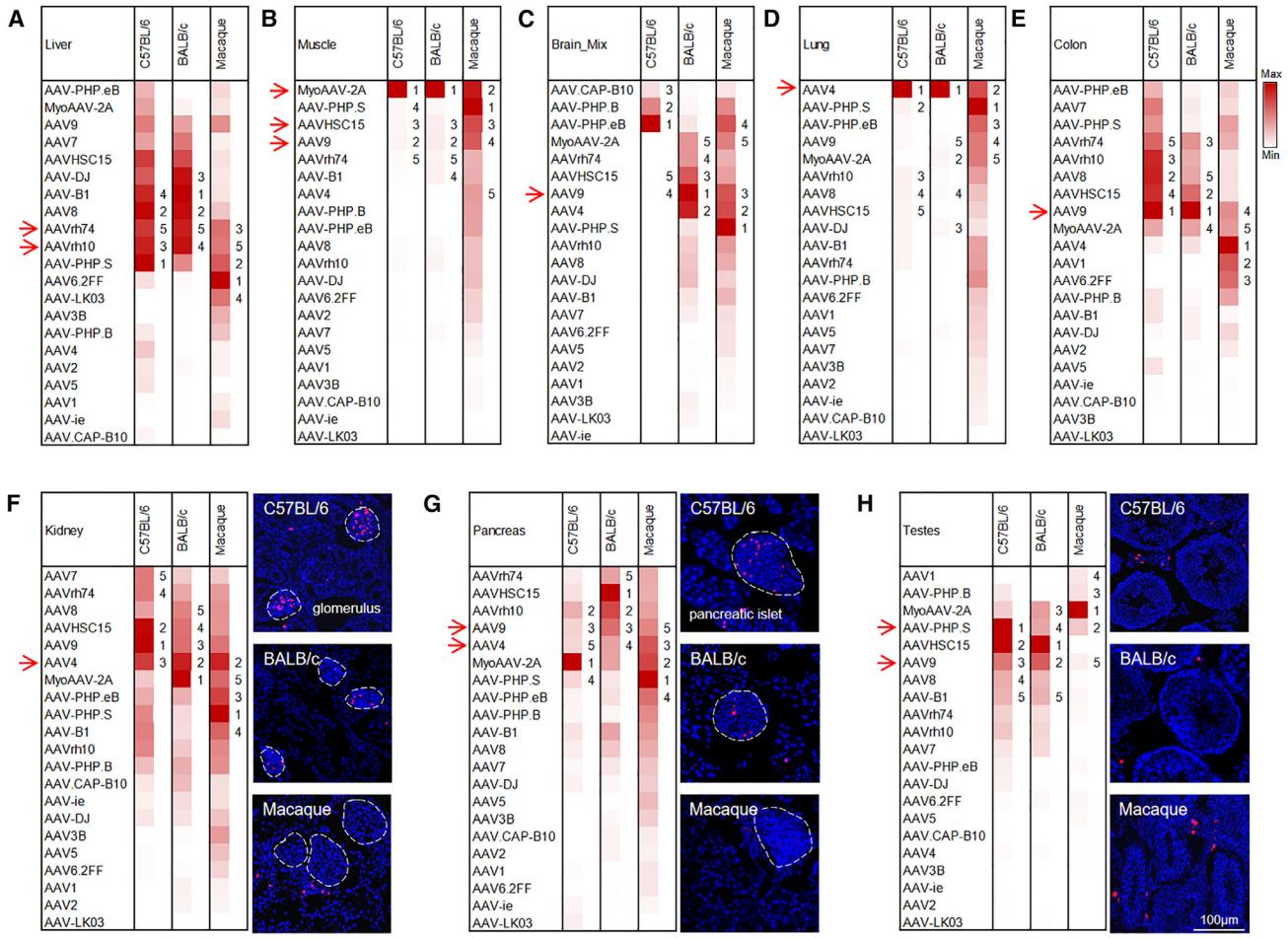

Figure 4. AAV capsid variants with the top transduction efficiencies across species

Heatmap of the RNA abundance of each AAV capsid in the liver (A), muscle (B), brain (C), lung (D), colon (E), kidney (F), pancreas (G), and testes (H). The RNA abundance of each capsid was calculated from the total RNA abundance of pooled AAVs. The RNA abundance of the macaque brain was averaged by the RNA abundance of 10 regions of the macaque brain. Numbers 1–5 represent the transduction rank of the AAV capsids in each tissue. The red arrow highlights the capsids that performed well across strains and species. Representative images of tdTomato expression in kidney (F), pancreas (G), and testes (H) are shown in the right panels. White dashed circles indicate the glomerulus in the kidneys (F) and the pancreatic islets in the pancreas (G), respectively.

summary, these findings offer an AAV capsid-selection profile for targeting specific tissues in both mice and macaques.

AAV4 exhibited liver-detargeting patterns in both mice and crab-eating macaques

Based on the exploration conducted using pooled AAVs and barcode sequencing, we identified AAV4 and AAV9 as the two most efficient capsid variants across multiple tissues. To validate these findings, we individually administered AAV4 and AAV9 intravenously to C57BL/6 mice or BALB/c mice at a dosage of 3E12 vg/kg (N = 3). The tropism of both capsids was evaluated 3 weeks after injection (Figures 5A and S5A).

Overall, we observed distinct patterns of vector DNA levels between AAV4 and AAV9 in mice. Notably, the vector DNA abundance of AAV9 was greatest in the liver among all 20 tissues. However, the vector DNA of AAV4 demonstrated a liver-detargeting pattern in both C57BL/6 and BALB/c mice, which was different from AAV9 (Figures 5B and S5B). Moreover, this liver-detargeting pattern of AAV4 infection was also evident in crab-eating macaques (Figures 5J and 5K).

Furthermore, we investigated the RNA expression of AAV4 and AAV9, observing distinct tropism between the two serotypes (Figure 5C). AAV9 demonstrated significantly greater transduction efficiency than AAV4 in the liver, brown adipose tissue, and testicular interstitium at both the RNA and protein levels (Figures 5C–5F). However, AAV4 displayed notably greater transduction efficiency in the lung, pancreatic islets, and glomerulus in C57BL/6 mice (Figures 5C and 5G–5I). For instance, the percentage of tdTomato$^+$

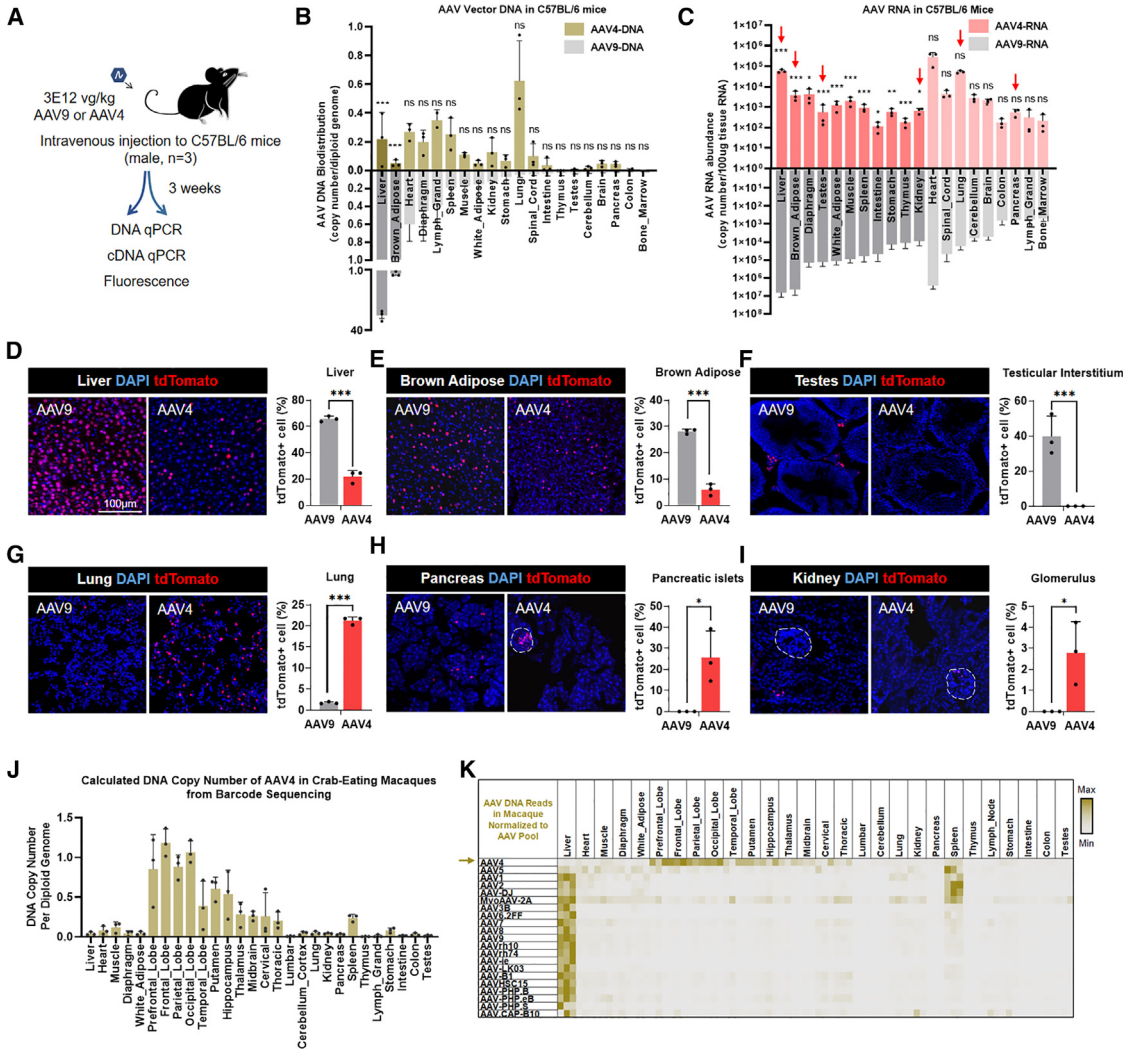

Figure 5. AAV4 exhibits different transduction patterns from AAV9 in C57BL/6 mice

(A) Schematic of the tropism analysis procedure for AAV4 and AAV9 in C57BL/6 mice. 3E12 vg/kg AAV4 or AAV9 was intravenously injected into mice (N = 3). The infection and transduction efficiency of the AAV pool was assessed at the DNA, RNA, and protein level. (B) Quantitative analysis of the vector DNA abundance of AAV4 and AAV9. N = 3; means ± SD; ns, not significant; ***$p < 0.001$; unpaired t tests. (C) Quantitative analysis of the vector RNA abundance of AAV4 and AAV9. N = 3; means ± SD; ns, not significant; *$p < 0.05$; **$p < 0.01$; ***$p < 0.001$; unpaired t tests. (D–I) Representative images of tdTomato expression delivered by AAV4 or AAV9 in tissues, including liver (D), brown adipose (E), testes (F), lung (G), pancreas (H), and kidney (I). The right graph shows the quantification of the tdTomato$^+$ cell proportion. N = 3; means ± SD; *$p < 0.05$; ***$p < 0.001$; unpaired t tests. White dashed circles indicate the glomerulus in the kidneys and the pancreatic islets in the pancreas respectively. (J) Quantitative analysis of the vector DNA abundance of AAV4 in crab-eating macaques. (K) Heatmap of the vector DNA abundance of each AAV capsid in crab-eating macaques. DNA abundance of each capsid was calculated from the total DNA abundance of the pooled AAVs and the proportion of each capsid.

cells in the lung was 21.23% ± 0.88% for AAV4 compared with 1.73% ± 0.24% for AAV9 ($p < 0.0001$) (Figure 5G). Additionally, significantly more tdTomato$^+$ cells were observed in the pancreatic islets and glomerulus with AAV4 (Figures 5H and 5I). These tropism differences between AAV4 and AAV9 were also evident in BALB/c mice (Figures S5C–S5I). In summary, AAV4 infection exhibited a unique liver-detargeting pattern in both mice and NHPs and demonstrated high effectiveness in transducing the lung, pancreatic islets, and glomerulus. These findings suggest the potential for developing capsids with low liver toxicity and new tropism properties based on AAV4.

DISCUSSION

Differences in AAV tropism have been noted across various strains or species.[22–26] However, there has been a lack of thorough investigations and comparisons of AAV tropism across species. To tackle this issue, our study aimed to explore the variations in AAV tropism across 21 capsid variants in C57BL/6 mice, BALB/c mice, and crab-eating macaques.

Our study systemically revealed noteworthy variations in AAV transduction among different mouse strains and between mice and

macaques. In comparison with C57BL/6 mice, BALB/c mice exhibited significantly lower transduction efficiencies in several certain tissues after the administration of pooled AAVs (Figure 1D), while crab-eating macaques showed lower transduction levels in most tissues (Figure 2C). Furthermore, diverse transduction patterns were observed among various AAV capsids across different strains or species. For instance, AAVHSC15, DJ, B1, and AAV8 demonstrated robust performance exclusively in the liver of mice, whereas AAV6.2FF and LK03 exhibited efficient transduction solely in the liver of macaques (Figure 4A). Therefore, our findings showed prevalent variations in AAV tropism across strains and species. Several factors may contribute to this inconsistency. First, variances in the expression of AAV receptors across strains or species could be one explanation. Previous research indicated that the ectopic expression of Ly6a might enhance the neurotropic properties of AAV-PHP.eB, resulting in high transduction rates specifically in C57BL/6 mice among seven tested mouse strains, but not in the remaining six strains.[23] Second, differences in host defense pathways and immune system would influence the AAV transfection between rodents and primates. In our study, we observed significantly higher vector DNA copies in the macaque spleen compared with mice (Figure 2B). Antigen presentation by antigen-presenting cells (APCs) may account for the differences in spleen DNA copy levels between mice and primates. Although we used immunosuppression reagents such as rituximab and rapamycin to suppress the post-AAV-infusion immune response, these treatments were unable to inhibit the antigen presentation by APCs, unlike corticosteroids. Additionally, pre-existing AAV NAbs against certain AAV capsid variants were detected in macaque serum (Table S1). The potential species-specific differences in pre-existing NAbs might influence the efficiency of AAV transduction between macaques and mice. Third, promoter selection[33] and endoplasmic reticulum stress in host cells[34] could influence AAV efficiency among species, according to previous reports. Based on these findings and hypotheses, some strategies such as modulating the immune system response, selecting appropriate promoters, adjusting translational elements, and enhancing AAV genome integration[25] could potentially enhance the efficiency and duration of AAV-mediated gene therapy in primates.

Moreover, we present a list of AAV capsid variants exhibiting high transduction efficiency in specific tissues of both mice and crab-eating macaques. For instance, AAV.rh10 and rh74 demonstrated efficacy in liver targeting in both species (Figure 4A), while MyoAAV-2A exhibited favorable performance in muscle targeting (Figure 4B), and AAV9 and HSC15 showed promise for brain targeting (Figure 4C). These findings align well with previous research, offering consistent evidence.[17,35–37] Additionally, novel insights emerged from our study. Previous research highlighted AAV6 and AAV8 as the most efficient capsid variants for transducing acinar cells or pancreatic islets in mouse pancreas among AAV1, AAV2, AAV5, AAV6, and AAV8.[38,39] Contrarily, we observed that AAV4 might outperform AAV6.2FF and AAV8 in transducing pancreas (Figure 4G). Notably, upon further intravenous administration of AAV4 to C57BL/6 mice and BALB/c mice, a pancreas-islet tropism was evident in AAV4 transduction (Figures 5H and S5H), indicating the potential of AAV4 for both research and therapeutic applications related to the pancreas. The specific cell type transduced by AAV4 in pancreatic islets warrants future investigation.

Furthermore, the investigation into the tropism of AAV4 unveiled its unique attributes among the tested capsid variants. A distinctive liver-detargeting characteristic and lung-tropic property of AAV4 have been observed in prior studies.[21,28] In our study, we found the liver-detargeting attribute of AAV4 was evident not only in mice, but also in macaques, setting it apart from the other 20 capsid variants examined in this study (Figures 5B, 5K, and S5B). In addition, we observed remarkable transduction efficiency of AAV4 in the lung, glomerulus, and pancreatic islets in both C57BL/6 and BALB/c mice (Figures 5G–5I and S5G–S5I). These unique tropisms of AAV may result from its specific structure. Previous studies have compared the structures of various wild-type capsids and noted the lowest correlation of AAV4 with other capsids.[40–42] Additionally, the receptor for AAV4 is O-linked carbohydrates of mucin, differing from receptors of other capsids.[43–46] These unique features likely contribute to the distinct tropism and liver-detargeting properties of AAV4, suggesting the potential for developing novel capsids with new tropism properties and reduced liver toxicity based on AAV4.

Limitations

(1) The reliability of barcode sequencing results may be compromised in tissues with low AAV transduction efficiency. This issue stems from our use of two sets of barcodes to assess sequencing robustness, revealing that sequencing outcomes lacked robustness when the initial PCR template was below 1E3 copies/reaction (Figure S1). In some macaque tissues, the initial cDNA copies hovered around 1E3 copies/reaction, potentially impacting the robustness of the barcode sequencing data.

(2) We used the ubiquitous CAG promoter to evaluate systemic AAV expression across multiple tissues. It is important to acknowledge that different promoters may influence AAV tropism results.[33] Future studies could explore the expression of AAVs driven by the tissue-specific and cell-specific promoters.

(3) Several novel AAV capsid variants with distinct tropism properties, such as 9P31,[47] MaCPNS1/MaCPNS2,[48] AAV-MG47,[49] and CPP.16,[50] were developed after the commencement of our study. Investigating the tropism profiles of these capsids could be a valuable avenue for future research.

(4) Pre-existing NAbs against AAV2, AAV5, AAV8, and AAV9 have estimated using Luciferase assay before AAV infusion. In our results, one macaque had an AAV2 NAb titer of greater than 1/660, and three macaques had an AAV8 NAb titer of greater than 1/66 (Table S1). Besides, a more systemic pre-existing NAb detection of 21 capsid variants was conducted using an NGS-based assay. We observed a 50% reduction in the vector-DNA-entry of capsid variants such as AAV2, 4, 5, DJ, and MyoAAV-2A, suggesting the presence of pre-existing AAV NAb in three macaques (Figure S6A). Due to the very limited possibility of selecting macaques without pre-existing antibodies against all AAV capsid

variants in macaques, we enrolled these macaques in our research. However, we must keep in mind that, since pre-existing NAbs might affect AAV transduction as mentioned before,[51] these different serotype-specific NAbs in the macaques studied here might affect the results we presented.

In summary, our investigation delved into the tropism profiles of multiple capsids across different strains and species, systematically exploring variations in AAV tropism between mice and macaques. We have compiled a list of suitable AAV capsids for targeted organ delivery, which holds potential significance for gene delivery and therapy targeting specific organs.

MATERIALS AND METHODS

Plasmids and barcodes

A series of barcoded AAV constructs were designed as ITR-barcode2-CAG-H2B-tdTomato-WPRE-Barcode1-SV40polyA-ITR. The sequences of 7nt-barcodes and corresponding AAV capsids are listed in Figures S1C and S1D.

AAV library production

Barcoded rAAVs were generated by the Gene Editing Facility at the Institute of Neuroscience using a standard polyethylenimine-based triple-plasmid co-transfection method in adherent HEK293T cells. We produced 21 AAV capsids, including AAV1-AAV9, rh10, rh74, DJ, i.e., LK03, B1, HSC15, PHP.B, PHP.eB, PHP.S, CAP-B10, and MyoAAV-2A. To increase the yield of AAV6, a triple-mutant variant named as AAV6.2FF was applied instead of AAV6.[46] The transfection reaction involved the Barcode2-CAG-H2B-tdTomato-WPRE-Barcode1-SV40polyA plasmids, pHelper, and corresponding pRep2Cap capsid plasmids, with a molar ratio of 1:1:1 (for a total of 40 μg/15-cm dish). Recombinant AAVs (rAAVs) were collected from both cell pellets and the media. The rAAVs from the cell pellets were released through a triple freeze/thaw process. The rAAVs from the media were precipitated using polyethylene glycol/NaCl. The titer of the raw AAV product for each harvested AAV capsid was determined using qPCR. To simplify the purification procedure and reduce the cost of AAV purification and production, all 21 AAV capsids were adjusted to the same copy number and mixed for iodixanol gradient centrifugation. The titer of the final AAV stock was assessed using a qPCR assay, while its purity was analyzed through SDS-PAGE and silver staining. The purity results of the mouse AAV library and NHP AAV library are shown in Figure S1. The composition of the barcoded capsid variants in the AAV library was determined by barcode sequencing. The composition results for the mouse and macaque AAV libraries are presented in Figure S1.

Additionally, other amounts of AAV4 and AAV9 were packaged and purified separately for administration to C57BL/6 and BALB/c mice for confirmation.

Animals

C57BL/6 and BALB/c mice were purchased from Vital River Laboratory Animal Technology Co., Ltd. Three male crab-eating macaques (*Macaca fascicularis*) were pre-screened for health status before study enrollment and housed in individual cages on a 12-h light/dark schedule in well-ventilated rooms (temperatures 18°C–29°C, humidity 40%–70%). Mouse protocol and macaque protocol were approved by the Biomedical Research Ethics Committee of the CAS Center for Excellence in Brain Science and Intelligence Technology, Chinese Academy of Sciences. Animal care complied with the guidelines of this committee.

AAV administration in mice

The mouse AAV library was suspended in 1× PBS containing 0.01% PF-68 to a concentrate of 1E12 vg/mL. Each 5-week-old male C57BL/6 and BALB/c mice were injected in the tail vein at an AAV dose of 5E12 vg/kg. The intravenous dose of separated AAV4 and AAV9 was 3E12 vg/kg.

AAV administration in crab-eating macaques

Three male crab-eating macaques were administrated with a pooled AAV injection. AAV pool was diluted in 1× PBS + 0.01% PF-68 to the concentration of 5E12 vg/mL, were slowly infused via the small saphenous vein injection. The total injection volume per animal was 1 mL/kg.

Before AAV injection, 4 mg/kg of an anesthetic (Zoletil) was injected for anesthesia. The detailed steps for injecting the small saphenous vein were as follows. First, cut local hair and disinfect with 75% ethanol, gripping the thigh with the hand until the small saphenous vein could be clearly seen. Second, hold a needle with a rubber tube attached to it in your right hand, and first insert the needle into the subcutaneous tissue adjacent to the blood vessel, then puncture the vein parallel to the blood vessel and connect the syringe to draw back. If blood returns, insert the needle tip a little further along the vascular lumen to remove the compression from the proximal end of the vein. Then, the injector holds the needle in place with one hand and slowly injects the solution into the vein at a rate of 1 mL/min.

To reduce a potential B cell-mediated immune reaction, 100 mg/kg of rituximab was injected via small saphenous vein 6 h before viral treatment and re-administrated every week. To suppress the T cell-mediated immune response, 2 mg/kg of rapamycin were given orally every day.

Three weeks after virus injection, NHPs were deeply anesthetized with 25 mg/kg of an anesthetic (Zoletil) and 100 μg/kg of Dextramer, and then perfused with cold PBS. Tissues were harvested for further investigation after 3 weeks after injection. All experiments were conducted by a qualified veterinarian.

Detection of NAb using luciferase

A cell-based transduction inhibition assay was used to determine NAb titers against AAV2, AAV5, AAV8, and AAV9 in serum samples by detecting luciferase expression. NAb assays followed a protocol adopted from a previous study[52] with some modifications. We

seeded 5 $\times 10^4$ of HEK293T cells in each well of a 48-well plate. Serum samples from the macaques collected before and 1, 2, and 3 weeks after AAV injection were initially diluted to 1:10, 1:33, 1:100, 1:330, and 1:1,000 in PBS. 10 μL of each serum dilution was mixed with 10 μL of AAV/CAG-Luciferase (5×10^3 VG/cell for AAV2 and AAV5, 10^4 VG/cell for AAV8, and 10^5 VG/cell for AAV9), and then incubated for 1 h at 37°C. The mixture was then added to the supernatant of 293T cells and incubated at 37°C with 5% CO_2. Fluorescence of firefly luciferase was detected after 48 h. NAb titers were reported as the interpolated serum dilution that produces 50% inhibition of the luciferase activity (ID_{50}) achieved in the absence of NHP serum.

Detection of NAb using NGS-based approach

A next-generation sequencing (NGS)-based transduction inhibition assay was used to assess the NAb titers using vector-DNA-entry as a readout. Five hundred thousand (5×10^5) HEK293T cells were seeded in each well of a 24-well plate. Serum samples from macaques, collected before and three weeks post-AAV injection, were initially diluted to concentrations of 1:10, 1:33, 1:100, 1:330, and 1:1,000 in PBS. Ten microliters of each serum dilution was mixed with 10 μL of the AAV library (1×10^3 viral genomes per cell), and the mixture was incubated at 37°C for 1 h. Subsequently, the mixture was added to the supernatant of the 293T cells and incubated at 37°C with 5% CO_2. After 48 h, total genomic DNA was extracted, amount of DNA entry of the total AAV library was assessed using qPCR, and amplicon sequencing was performed to determine the copy number of each AAV capsid variant. NAb titers were expressed as the ID_{50} that resulted in a 50% inhibition of DNA entry compared with the absence of NHP serum.

Extraction of DNA and RNA

DNA of AAV pool or tissues was extracted using DNeasy Blood & Tissue Kit (Qiagen). Briefly, to extract AAV genome, 1E11 vg of AAV pool was incubated with DNase I at 37°C for 30 min, heated to 98°C for 30 min, and extracted following the manufacturer's protocol. To extract DNA from mouse and NHP tissues, 10 mg tissue was homogenate in ATL buffer, and then extracted following the manufacturer's protocol.

To extract RNA from tissues, 30 mg tissue was dissected and kept in RNAlater at −80°C overnight. Then tissues were homogenated in Trizol (Invitrogen 15596026CN) and extracted following the user guide of Trizol. CDNA were synthesized using the HiScript Q RT SuperMix for qPCR Kit (Vazyme).

Real-time qPCR

For quantification of the viral DNA and cDNA amount in each sample, we used Taqmen qPCR with a primer and probe set targeting the WPRE element. For each sample, Taqmen quantitative real-time PCR was performed by Bestar qPCR Master Mix (DBI), using 100 ng of gDNA or cDNA (equivalent of 100 ng total RNA) as template. The cycle threshold value for each sample was used to assess relative barcoded vector content. The DNA abundance was normalized to mouse and macaque Gapdh fragment. All the Taqman primer and probe sets were listed in Table S2.

Histology and immunostaining

For mice and NHPs, tissues were fixed in 4% PFA for more than 24 h, then dehydrated in 30% sucrose and imbedded in the optimal cutting temperature compound for frozen sectioning. We prepared 20-μm-thick sections, stained with DAPI and imaged using confocal microscopy (Olympus FV3000).

Barcode sequencing and bioinformatics analysis

Amplification of DNA and cDNA fragments for barcode screening was carried out using the Phanta Max Super-Fidelity DNA Polymerase (Vazyme) for 35 cycles. Each sample was amplified using a pair of primers with unique external index. The PCR primer sequences can be found in Table S2. Sequencing of the NGS library was performed using the NextSeq 500 HC instrument. For the bioinformatics analysis, the reads from different tissues were identified using the external index of each primer pair. The AAV composition of each sample was normalized to the NGS reference of the injected AAV pool. The distribution of the separated AAV vectors and the abundance of RNA were calculated by multiplying the AAV composition with the DNA and RNA abundance of the entire AAV pool.

DATA AVAILABILITY

The authors confirm that the data supporting the findings of this study are available within the article and in supplemental information.

ACKNOWLEDGMENTS

This study was supported by the Basic Frontier Scientific Research Program of Chinese Academy of Sciences from 0 to 1 original innovation project (ZDBS-LY-SM001), National Science and Technology Innovation 2030 Major Program (2021ZD0200900), National Natural Science Foundation of China (31925016, 82021001), and Project of Shanghai Municipal Science and Technology Commission (20MC1920400).

AUTHOR CONTRIBUTIONS

K.F., G.G., L.S., and H.Y. conceived and designed the research. K.F., G.G., X.Y., J.X., R.W., X.L., and C.F. conducted experiments and analyzed data. Y.L. performed barcode sequencing analysis. K.F., G.G., and H.Y. wrote the manuscript with input from all authors.

DECLARATION OF INTERESTS

H.Y. and L.Sv are co-founders of Huidagene Therapeutics Co., Ltd. J.X. and R.W. are employees of Huidagene Therapeutics Co.

SUPPLEMENTAL INFORMATION

Supplemental information can be found online at https://doi.org/10.1016/j.omtm.2025.101434.

REFERENCES

1. Atchison, R.W., Casto, B.C., and Hammon, W.M. (1965). Adenovirus-Associated Defective Virus Particles. Science *149*, 754–756. https://doi.org/10.1126/science.149.3685.754.

2. Pasi, K.J., Rangarajan, S., Mitchell, N., Lester, W., Symington, E., Madan, B., Laffan, M., Russell, C.B., Li, M., Pierce, G.F., and Wong, W.Y. (2020). Multiyear Follow-up of AAV5-hFVIII-SQ Gene Therapy for Hemophilia A. N. Engl. J. Med. *382*, 29–40. https://doi.org/10.1056/NEJMoa1908490.

3. Mendell, J.R., Al-Zaidy, S., Shell, R., Arnold, W.D., Rodino-Klapac, L.R., Prior, T.W., Lowes, L., Alfano, L., Berry, K., Church, K., et al. (2017). Single-Dose Gene-Replacement Therapy for Spinal Muscular Atrophy. N. Engl. J. Med. *377*, 1713–1722. https://doi.org/10.1056/NEJMoa1706198.

4. Tai, C.H., Lee, N.C., Chien, Y.H., Byrne, B.J., Muramatsu, S.I., Tseng, S.H., and Hwu, W.L. (2022). Long-term efficacy and safety of eladocagene exuparvovec in patients with AADC deficiency. Mol. Ther. *30*, 509–518. https://doi.org/10.1016/j.ymthe.2021.11.005.

5. Bennett, J., Wellman, J., Marshall, K.A., McCague, S., Ashtari, M., DiStefano-Pappas, J., Elci, O.U., Chung, D.C., Sun, J., Wright, J.F., et al. (2016). Safety and durability of effect of contralateral-eye administration of AAV2 gene therapy in patients with childhood-onset blindness caused by RPE65 mutations: a follow-on phase 1 trial. Lancet *388*, 661–672. https://doi.org/10.1016/S0140-6736(16)30371-3.

6. Mendell, J.R., Sahenk, Z., Lehman, K., Nease, C., Lowes, L.P., Miller, N.F., Iammarino, M.A., Alfano, L.N., Nicholl, A., Al-Zaidy, S., et al. (2020). Assessment of Systemic Delivery of rAAVrh74.MHCK7.micro-dystrophin in Children With Duchenne Muscular Dystrophy: A Nonrandomized Controlled Trial. JAMA Neurol. *77*, 1122–1131. https://doi.org/10.1001/jamaneurol.2020.1484.

7. Gaudet, D., Méthot, J., Déry, S., Brisson, D., Essiembre, C., Tremblay, G., Tremblay, K., de Wal, J., Twisk, J., van den Bulk, N., et al. (2013). Efficacy and long-term safety of alipogene tiparvovec (AAV1-LPLS447X) gene therapy for lipoprotein lipase deficiency: an open-label trial. Gene Ther. *20*, 361–369. https://doi.org/10.1038/gt.2012.43.

8. Miesbach, W., Meijer, K., Coppens, M., Kampmann, P., Klamroth, R., Schutgens, R., Tangelder, M., Castaman, G., Schwäble, J., Bonig, H., et al. (2018). Gene therapy with adeno-associated virus vector 5-human factor IX in adults with hemophilia B. Blood *131*, 1022–1031. https://doi.org/10.1182/blood-2017-09-804419.

9. Grimm, D., Lee, J.S., Wang, L., Desai, T., Akache, B., Storm, T.A., and Kay, M.A. (2008). In vitro and *in vivo* gene therapy vector evolution via multispecies interbreeding and retargeting of adeno-associated viruses. J. Virol. *82*, 5887–5911. https://doi.org/10.1128/jvi.00254-08.

10. Petrs-Silva, H., Dinculescu, A., Li, Q., Deng, W.T., Pang, J.J., Min, S.H., Chiodo, V., Neeley, A.W., Govindasamy, L., Bennett, A., et al. (2011). Novel properties of tyrosine-mutant AAV2 vectors in the mouse retina. Mol. Ther. *19*, 293–301. https://doi.org/10.1038/mt.2010.234.

11. Lisowski, L., Dane, A.P., Chu, K., Zhang, Y., Cunningham, S.C., Wilson, E.M., Nygaard, S., Grompe, M., Alexander, I.E., and Kay, M.A. (2014). Selection and evaluation of clinically relevant AAV variants in a xenograft liver model. Nature *506*, 382–386. https://doi.org/10.1038/nature12875.

12. Smith, L.J., Ul-Hasan, T., Carvaines, S.K., Van Vliet, K., Yang, E., Wong, K.K., Jr., Agbandje-McKenna, M., and Chatterjee, S. (2014). Gene transfer properties and structural modeling of human stem cell-derived AAV. Mol. Ther. *22*, 1625–1634. https://doi.org/10.1038/mt.2014.107.

13. Choudhury, S.R., Fitzpatrick, Z., Harris, A.F., Maitland, S.A., Ferreira, J.S., Zhang, Y., Ma, S., Sharma, R.B., Gray-Edwards, H.L., Johnson, J.A., et al. (2016). In Vivo Selection Yields AAV-B1 Capsid for Central Nervous System and Muscle Gene Therapy. Mol. Ther. *24*, 1247–1257. https://doi.org/10.1038/mt.2016.84.

14. Deverman, B.E., Pravdo, P.L., Simpson, B.P., Kumar, S.R., Chan, K.Y., Banerjee, A., Wu, W.L., Yang, B., Huber, N., Pasca, S.P., and Gradinaru, V. (2016). Cre-dependent selection yields AAV variants for widespread gene transfer to the adult brain. Nat. Biotechnol. *34*, 204–209. https://doi.org/10.1038/nbt.3440.

15. Landegger, L.D., Pan, B., Askew, C., Wassmer, S.J., Gluck, S.D., Galvin, A., Taylor, R., Forge, A., Stankovic, K.M., Holt, J.R., and Vandenberghe, L.H. (2017). A synthetic AAV vector enables safe and efficient gene transfer to the mammalian inner ear. Nat. Biotechnol. *35*, 280–284. https://doi.org/10.1038/nbt.3781.

16. Chan, K.Y., Jang, M.J., Yoo, B.B., Greenbaum, A., Ravi, N., Wu, W.L., Sánchez-Guardado, L., Lois, C., Mazmanian, S.K., Deverman, B.E., and Gradinaru, V. (2017). Engineered AAVs for efficient noninvasive gene delivery to the central and peripheral nervous systems. Nat. Neurosci. *20*, 1172–1179. https://doi.org/10.1038/nn.4593.

17. Tabebordbar, M., Lagerborg, K.A., Stanton, A., King, E.M., Ye, S., Tellez, L., Krunnfusz, A., Tavakoli, S., Widrick, J.J., Messemer, K.A., et al. (2021). Directed evolution of a family of AAV capsid variants enabling potent muscle-directed gene delivery across species. Cell *184*, 4919–4938.e22. https://doi.org/10.1016/j.cell.2021.08.028.

18. Goertsen, D., Flytzanis, N.C., Goeden, N., Chuapoco, M.R., Cummins, A., Chen, Y., Fan, Y., Zhang, Q., Sharma, J., Duan, Y., et al. (2022). AAV capsid variants with brain-wide transgene expression and decreased liver targeting after intravenous delivery in mouse and marmoset. Nat. Neurosci. *25*, 106–115. https://doi.org/10.1038/s41593-021-00969-4.

19. Adachi, K., Enoki, T., Kawano, Y., Veraz, M., and Nakai, H. (2014). Drawing a high-resolution functional map of adeno-associated virus capsid by massively parallel sequencing. Nat. Commun. *5*, 3075. https://doi.org/10.1038/ncomms4075.

20. Marsic, D., Méndez-Gómez, H.R., and Zolotukhin, S. (2015). High-accuracy biodistribution analysis of adeno-associated virus variants by double barcode sequencing. Mol. Ther. Methods Clin. Dev. *2*, 15041. https://doi.org/10.1038/mtm.2015.41.

21. Zincarelli, C., Soltys, S., Rengo, G., and Rabinowitz, J.E. (2008). Analysis of AAV serotypes 1-9 mediated gene expression and tropism in mice after systemic injection. Mol. Ther. *16*, 1073–1080. https://doi.org/10.1038/mt.2008.76.

22. Hordeaux, J., Wang, Q., Katz, N., Buza, E.L., Bell, P., and Wilson, J.M. (2018). The Neurotropic Properties of AAV-PHP.B Are Limited to C57BL/6J Mice. Mol. Ther. *26*, 664–668. https://doi.org/10.1016/j.ymthe.2018.01.018.

23. Huang, Q., Chan, K.Y., Tobey, I.G., Chan, Y.A., Poterba, T., Boutros, C.L., Balazs, A.B., Daneman, R., Bloom, J.M., Seed, C., and Deverman, B.E. (2019). Delivering genes across the blood-brain barrier: LY6A, a novel cellular receptor for AAV-PHP.B capsids. PLoS One *14*, e0225206. https://doi.org/10.1371/journal.pone.0225206.

24. Cunningham, S.C., Dane, A.P., Spinoulas, A., Alexander, I.E., and Alexander, I.E. (2008). Gene delivery to the juvenile mouse liver using AAV2/8 vectors. Mol. Ther. *16*, 1081–1088. https://doi.org/10.1038/mt.2008.72.

25. Greig, J.A., Martins, K.M., Breton, C., Lamontagne, R.J., Zhu, Y., He, Z., White, J., Zhu, J.X., Chichester, J.A., Zheng, Q., et al. (2024). Integrated vector genomes may contribute to long-term expression in primate liver after AAV administration. Nat. Biotechnol. *42*, 1232–1242. https://doi.org/10.1038/s41587-023-01974-7.

26. Hurlbut, G.D., Ziegler, R.J., Nietupski, J.B., Foley, J.W., Woodworth, L.A., Meyers, E., Bercury, S.D., Pande, N.N., Souza, D.W., Bree, M.P., et al. (2010). Preexisting immunity and low expression in primates highlight translational challenges for liver-directed AAV8-mediated gene therapy. Mol. Ther. *18*, 1983–1994. https://doi.org/10.1038/mt.2010.175.

27. Nathwani, A.C., Rosales, C., McIntosh, J., Rastegarlari, G., Nathwani, D., Raj, D., Nawathe, S., Waddington, S.N., Bronson, R., Jackson, S., et al. (2011). Long-term safety and efficacy following systemic administration of a self-complementary AAV vector encoding human FIX pseudotyped with serotype 5 and 8 capsid proteins. Mol. Ther. *19*, 876–885. https://doi.org/10.1038/mt.2010.274.

28. Westhaus, A., Cabanes-Creus, M., Rybicki, A., Baltazar, G., Navarro, R.G., Zhu, E., Drouyer, M., Knight, M., Albu, R.F., Ng, B.H., et al. (2020). High-Throughput In Vitro, Ex Vivo, and In Vivo Screen of Adeno-Associated Virus Vectors Based on Physical and Functional Transduction. Hum. Gene Ther. *31*, 575–589. https://doi.org/10.1089/hum.2019.264.

29. Weinmann, J., Weis, S., Sippel, J., Tulalamba, W., Remes, A., El Andari, J., Herrmann, A.K., Pham, Q.H., Borowski, C., Hille, S., et al. (2020). Identification of a myotropic AAV by massively parallel *in vivo* evaluation of barcoded capsid variants. Nat. Commun. *11*, 5432. https://doi.org/10.1038/s41467-020-19230-w.

30. Mingozzi, F., Hasbrouck, N.C., Basner-Tschakarjan, E., Edmonson, S.A., Hui, D.J., Sabatino, D.E., Zhou, S., Wright, J.F., Jiang, H., Pierce, G.F., et al. (2007). Modulation of tolerance to the transgene product in a nonhuman primate model of AAV-mediated gene transfer to liver. Blood *110*, 2334–2341. https://doi.org/10.1182/blood-2007-03-080093.

31. Mingozzi, F., Chen, Y., Murphy, S.L., Edmonson, S.C., Tai, A., Price, S.D., Metzger, M.E., Zhou, S., Wright, J.F., Donahue, R.E., et al. (2012). Pharmacological modulation of humoral immunity in a nonhuman primate model of AAV gene transfer for hemophilia B. Mol. Ther. *20*, 1410–1416. https://doi.org/10.1038/mt.2012.84.

32. Unzu, C., Hervás-Stubbs, S., Sampedro, A., Mauleón, I., Mancheño, U., Alfaro, C., de Salamanca, R.E., Benito, A., Beattie, S.G., Petry, H., et al. (2012). Transient and intensive pharmacological immunosuppression fails to improve AAV-based liver gene

transfer in non-human primates. J. Transl. Med. *10*, 122. https://doi.org/10.1186/1479-5876-10-122.

33. Nakai, H., Herzog, R.W., Hagstrom, J.N., Walter, J., Kung, S.H., Yang, E.Y., Tai, S.J., Iwaki, Y., Kurtzman, G.J., Fisher, K.J., et al. (1998). Adeno-associated viral vector-mediated gene transfer of human blood coagulation factor IX into mouse liver. Blood *91*, 4600–4607.

34. Zolotukhin, I., Markusic, D.M., Palaschak, B., Hoffman, B.E., Srikanthan, M.A., and Herzog, R.W. (2016). Potential for cellular stress response to hepatic factor VIII expression from AAV vector. Mol. Ther. Methods Clin. Dev. *3*, 16063. https://doi.org/10.1038/mtm.2016.63.

35. Ellsworth, J.L., Gingras, J., Smith, L.J., Rubin, H., Seabrook, T.A., Patel, K., Zapata, N., Olivieri, K., O'Callaghan, M., Chlipala, E., et al. (2019). Clade F AAVHSCs cross the blood brain barrier and transduce the central nervous system in addition to peripheral tissues following intravenous administration in nonhuman primates. PLoS One *14*, e0225582. https://doi.org/10.1371/journal.pone.0225582.

36. Foust, K.D., Nurre, E., Montgomery, C.L., Hernandez, A., Chan, C.M., and Kaspar, B.K. (2009). Intravascular AAV9 preferentially targets neonatal neurons and adult astrocytes. Nat. Biotechnol. *27*, 59–65. https://doi.org/10.1038/nbt.1515.

37. Mattar, C.N., Waddington, S.N., Biswas, A., Johana, N., Ng, X.W., Fisk, A.S., Fisk, N.M., Tan, L.G., Rahim, A.A., Buckley, S.M.K., et al. (2013). Systemic delivery of scAAV9 in fetal macaques facilitates neuronal transduction of the central and peripheral nervous systems. Gene Ther. *20*, 69–83. https://doi.org/10.1038/gt.2011.216.

38. Wang, A.Y., Peng, P.D., Ehrhardt, A., Storm, T.A., and Kay, M.A. (2004). Comparison of adenoviral and adeno-associated viral vectors for pancreatic gene delivery *in vivo*. Hum. Gene Ther. *15*, 405–413. https://doi.org/10.1089/104303404322959551.

39. Wang, Z., Zhu, T., Rehman, K.K., Bertera, S., Zhang, J., Chen, C., Papworth, G., Watkins, S., Trucco, M., Robbins, P.D., et al. (2006). Widespread and stable pancreatic gene transfer by adeno-associated virus vectors via different routes. Diabetes *55*, 875–884. https://doi.org/10.2337/diabetes.55.04.06.db05-0927.

40. Govindasamy, L., Padron, E., McKenna, R., Muzyczka, N., Kaludov, N., Chiorini, J.A., and Agbandje-McKenna, M. (2006). Structurally mapping the diverse phenotype of adeno-associated virus serotype 4. J. Virol. *80*, 11556–11570. https://doi.org/10.1128/jvi.01536-06.

41. Mietzsch, M., Jose, A., Chipman, P., Bhattacharya, N., Daneshparvar, N., McKenna, R., and Agbandje-McKenna, M. (2021). Completion of the AAV Structural Atlas: Serotype Capsid Structures Reveals Clade-Specific Features. Viruses *13*, 101. https://doi.org/10.3390/v13010101.

42. Padron, E., Bowman, V., Kaludov, N., Govindasamy, L., Levy, H., Nick, P., McKenna, R., Muzyczka, N., Chiorini, J.A., Baker, T.S., and Agbandje-McKenna, M. (2005). Structure of adeno-associated virus type 4. J. Virol. *79*, 5047–5058. https://doi.org/10.1128/jvi.79.8.5047-5058.2005.

43. Dudek, A.M., Pillay, S., Puschnik, A.S., Nagamine, C.M., Cheng, F., Qiu, J., Carette, J.E., and Vandenberghe, L.H. (2018). An Alternate Route for Adeno-associated Virus (AAV) Entry Independent of AAV Receptor. J. Virol. *92*, e02213-17. https://doi.org/10.1128/jvi.02213-17.

44. Kaludov, N., Brown, K.E., Walters, R.W., Zabner, J., and Chiorini, J.A. (2001). Adeno-associated virus serotype 4 (AAV4) and AAV5 both require sialic acid binding for hemagglutination and efficient transduction but differ in sialic acid linkage specificity. J. Virol. *75*, 6884–6893. https://doi.org/10.1128/jvi.75.15.6884-6893.2001.

45. Shen, S., Troupes, A.N., Pulicherla, N., and Asokan, A. (2013). Multiple roles for sialylated glycans in determining the cardiopulmonary tropism of adeno-associated virus 4. J. Virol. *87*, 13206–13213. https://doi.org/10.1128/jvi.02109-13.

46. Walters, R.W., Pilewski, J.M., Chiorini, J.A., and Zabner, J. (2002). Secreted and transmembrane mucins inhibit gene transfer with AAV4 more efficiently than AAV5. J. Biol. Chem. *277*, 23709–23713. https://doi.org/10.1074/jbc.M200292200.

47. Nonnenmacher, M., Wang, W., Child, M.A., Ren, X.Q., Huang, C., Ren, A.Z., Tocci, J., Chen, Q., Bittner, K., Tyson, K., et al. (2021). Rapid evolution of blood-brain-barrier-penetrating AAV capsids by RNA-driven biopanning. Mol. Ther. Methods Clin. Dev. *20*, 366–378. https://doi.org/10.1016/j.omtm.2020.12.006.

48. Chen, X., Ravindra Kumar, S., Adams, C.D., Yang, D., Wang, T., Wolfe, D.A., Arokiaraj, C.M., Ngo, V., Campos, L.J., Griffiths, J.A., et al. (2022). Engineered AAVs for non-invasive gene delivery to rodent and non-human primate nervous systems. Neuron *110*, 2242–2257.e6. https://doi.org/10.1016/j.neuron.2022.05.003.

49. Lin, R., Zhou, Y., Yan, T., Wang, R., Li, H., Wu, Z., Zhang, X., Zhou, X., Zhao, F., Zhang, L., et al. (2022). Directed evolution of adeno-associated virus for efficient gene delivery to microglia. Nat. Methods *19*, 976–985. https://doi.org/10.1038/s41592-022-01547-7.

50. Yao, Y., Wang, J., Liu, Y., Qu, Y., Wang, K., Zhang, Y., Chang, Y., Yang, Z., Wan, J., Liu, J., et al. (2022). Variants of the adeno-associated virus serotype 9 with enhanced penetration of the blood-brain barrier in rodents and primates. Nat. Biomed. Eng. *6*, 1257–1271. https://doi.org/10.1038/s41551-022-00938-7.

51. Wang, L., Calcedo, R., Bell, P., Lin, J., Grant, R.L., Siegel, D.L., and Wilson, J.M. (2011). Impact of pre-existing immunity on gene transfer to nonhuman primate liver with adeno-associated virus 8 vectors. Hum. Gene Ther. *22*, 1389–1401. https://doi.org/10.1089/hum.2011.031.

52. Calcedo, R., Vandenberghe, L.H., Gao, G., Lin, J., and Wilson, J.M. (2009). Worldwide epidemiology of neutralizing antibodies to adeno-associated viruses. J. Infect. Dis. *199*, 381–390. https://doi.org/10.1086/595830.